ResearchGate

See discussions, stats, and author profiles for this publication at: https://www.researchgate.net/publication/231274363

Asphaltene-Induced Precipitation and Deposition During Pressure Depletion on a Porous Medium: An Experimental Investigation and Modeling Approach

ARTICLE *in* ENERGY & FUELS · NOVEMBER 2009

Impact Factor: 2.79 · DOI: 10.1021/ef9006142

CITATIONS
8

READS
78

5 AUTHORS, INCLUDING:

Francisco Arguelles Vivas
University of Texas at Austin
9 PUBLICATIONS **21** CITATIONS
SEE PROFILE

S. López-Ramírez
Universidad Nacional Autónoma de México
26 PUBLICATIONS **250** CITATIONS
SEE PROFILE

Available from: Francisco Arguelles Vivas
Retrieved on: 01 February 2016

Energy Fuels **2009,** *23,* 5611–5625 · DOI:10.1021/ef9006142
Published on Web 10/01/2009

energy&fuels
article

Asphaltene-Induced Precipitation and Deposition During Pressure Depletion on a Porous Medium: An Experimental Investigation and Modeling Approach

José L. Mendoza de la Cruz,*,† Francisco J. Argüelles-Vivas,‖ Víctor Matías-Pérez,⊥ Cecilia de los A. Durán-Valencia,§ and Simón López-Ramírez‡

†*Coordinación de Investigación y Desarrollo Tecnológico de Aseguramiento de la Producción de Hidrocarburos,* ‡*Coordinación de Ingeniería Molecular,* §*Coordinación de Recuperación de Hidrocarburos. Instituto Mexicano del Petróleo, Eje Central Lázaro Cárdenas Norte 152, Col. San Bartolo Atepehuacan, Del. Gustavo A. Madero, 07730, Mexico, D. F., Mexico,* ‖ *Universidad Autónoma Metropolitana-Azcapotzalco, CBI, Área de Energía, Av. San Pablo 180, Col. Reynosa Tamaulipas, 02200, Mexico, D. F. Mexico, and* ⊥*Universidad Nacional Autónoma de México, DEPFI, Apartado Postal 70-256, Av. Insurgentes Sur s/n, Cd. Universitaria, 04510, Del. Coyoacán, Mexico, D. F. Mexico*

Received June 17, 2009. Revised Manuscript Received September 1, 2009

Dynamic displacement experiments, simulating temperature and pressure conditions of an oil-bearing formation during primary production stage, were carried out to investigate the processes of asphaltene-induced precipitation and deposition during pressure depletion on a core sample and their effects on the absolute permeability. A representative monophasic-bottom-hole fluid sample and one core of consolidated Bedford limestone were used in coreflood tests. To identify the pressure and temperature conditions at which the asphaltene will begin to precipitate, as well as the bubble-point pressures of the reservoir fluid sample, the light-scattering technique solid detection system (SDS) using a variable volume, visual *PVT* cell was used. The coreflood test results indicated that the in situ asphaltene precipitation and deposition on porous medium damage absolute permeability and reduce effective porosity as reservoir fluid pressure is reduced until a point near bubble-point pressure. Core impairment, resulting from asphaltene deposition, was found to cause a 24% and 20% loss of initial oil permeability and effective porosity, respectively. A mathematical model, based on the transport of stable particulate suspensions in porous media, for asphaltene deposition was developed and validated directly with experimental results obtained in this investigation, as well as those found in the literature. On the basis of the developed mathematical model, two distinct mechanisms were identified as a consequence of the deposition process, namely, asphaltene adsorption and trapping. The porous medium was represented as a network of sites and bonds, with pore bodies identified as sites and pore throats as bonds. A satisfactory qualitative agreement was observed with the experimental results.

1. Introduction and Review

The processes of asphaltene precipitation and deposition in porous media have a substantial effect on oil flow during primary oil production and enhanced oil recovery processes;[1−11] it is well-known that during primary production stage of a reservoir, oil flows through regions with the minor resistance (i.e., porous matrix and fractures), and the impulse force arising the fluids movement between the porous spaces of rock is a pressure difference in the rock−fluid system. The natural depletion of a reservoir may cause the precipitation

*To whom correspondence should be addressed. E-mail: jlmendoz@imp.mx. Telephone: +52-55-91-75-65-03.

(1) Lichaa, P. M.; Herrera, L. Electrical and other effects related to the formation and prevention of asphaltene deposition. In SPE of AIME 5304 presented at the International Symposium on Oilfield Chemistry in Dallas, Texas, Jan 16−17, 1975; p 107.
(2) Tuttle, R. N. *J. Pet. Technol.* **1983**, 1192–1196.
(3) Newberry, M. E.; Barker, K. M. Formation damage prevention through the control of paraffin and asphaltene deposition. In SPE 13796 presented at the Production Operations Symposium held in Oklahoma City, Oklahoma, March 10−12, 1985; p 53.
(4) Leontaritis, K. J.; Mansoori, G. A., Asphaltene flocculation during oil production and processing: A thermodynamic colloidal model. In SPE 16258 presented at the International Symposium on Oilfield Chemistry in San Antonio, Texas, Feb 4−6, 1987; p 149.
(5) Leontaritis, K. J.; Kawanaka, S.; Mansoori, G. A. Descriptive accounts of thermodynamic and colloidal models of asphaltene flocculation. In Symposium on Advances in Oil Field Chemistry presented before the division of Petroleum Chemistry, Inc., American Chemical Society, Toronto Meeting, June 5−11, 1988; pp 196−204.
(6) Leontaritis, K. J.; Mansoori, G. A. *J. Pet. Sci. Eng.* **1988**, *1*, 229–239.
(7) Leontaritis, K. J. Asphaltene deposition: A comprehensive description of problem manifestations and modeling approaches. In SPE 18892 presented at the SPE Production Operations Symposium held in Oklahoma, City, OK, March 13−14, 1989; p 229.
(8) Islam, M. R. In *Asphaltenes and Asphalts, Developments in Petroleum Science*; Yen, T. F., Chilingarian, G. V. Eds.; Elsevier: Amsterdan, 1994; Vol. 40, Chap. 11.
(9) Leontaritis, K. J.; Amaefule, J. O.; Charles, R. E. A systematic approach for the prevention and treatment of formation damage caused by asphaltene deposition. In *SPE Production and Facilities*, 1994; pp 157−164.
(10) Kokal, S. L.; Sayegh, S. G., Asphaltenes: The cholesterol of petroleum. In SPE 29787 presented at the SPE Middle East Oil Show held in Bahrain, March 11−14, 1995; p 169.
(11) Civan, F., Reservoir formation damage *Fundamentals, Modeling, Assessment, and Mitigation*, 1st. ed.; Gulf Publishing Company: Houston, TX, 2000; p 742.
(12) Haskett, C. E.; Tartera, M. *J. Pet. Technol.* **1965**, *17*, 387–391.
(13) Minssieux, L., Core damage from crude asphaltene deposition. In SPE 37250 presented at the SPE International Symposium on Oilfield Chemistry held in Houston, Texas, February 18−21, 1997; p 401.
(14) Ali, M. A.; Islam, M. R. The effect of asphaltene precipitation on carbonate rock permeability: An experimental and numerical approach. In SPE 38856 presented at SPE Annual Technical Conference and Exhibition held in San Antonio, October 5−6, 1997; p 139.

© 2009 American Chemical Society

and flocculation phenomena of organic solids (asphaltenes or waxes) diminishing the productivity of well during primary oil recovery.[1,2,5,12−20]

In general, field experiences[1−4,6−10,12,21−27] and laboratory tests on coreflooding[1,13−20,28−34] have demonstrated that any operation carried out in the oilfield (i.e., drilling, cementation, completion, workover, production, injection of fluid, acid stimulation, and hydraulic fracturing) is a potential source of damage to well productivity. Although the way in which well productivity may be damaged varies from operation to operation, the researches and diagnosis of specific problems have led to the conclusion that formation damage is usually associated with the transport of fine solids, chemical reactions, and thermodynamic considerations.[5,22,30]

Particularly, during the stage of primary oil production, one of the common sources of plugging in the porous space of the rock formation is displacement of organic material (fines solids) from crude oil contained in the oil-bearing formation as the reservoir natural depletion proceeds. Although production rates usually decline with the natural depletion of a field, accelerated decline from formation plugging is a common problem during production operations that must be dealt with to maintain an adequate return on investment.[22] It is well-known that petroleum is a source of plugging organic materials (i.e., asphaltenes, waxes, and/or paraffins), and once they separate from crude oil may cause obstruction in the flow path. In general, asphaltenes are considered the most aromatic and polar fraction in the crude oil. Initially, it is believed that these molecules are homogeneously distributed or dissolved in crude oil at a stable condition. However, when oil reservoirs are produced, alteration of oil conditions by various recovery methods may render asphaltene unstable and precipitate from the crude oil.[9,30]

Essentially, three main factors affect the asphaltene precipitation in reservoirs during oil recovery: reservoir pressure, temperature, and oil composition.[2,5,12,14,30,35,36] Considering there is no injection of fluid into the oil reservoir and temperature is assumed to be constant, decline of pressure (due to reservoir natural depletion) is the major factor that causes the asphaltene precipitation in reservoirs during the primary oil recovery. Thus, the precipitation and its subsequent deposition process of this kind of material as a consequence of primary depletion, under isothermal conditions, are preferentially of the asphaltene types.[9,20,30,37,38]

Generally, organic aggregates from crude oil appear first in surface facilities, especially in separation stages, during the crude oil final depressurization step.[5,9,39,40] Another critical point in the petroleum production chain is in tubing string in which deposits form at depths where the crude oil reaches pressures around its bubble-point pressure.[2,12,13,15,41] Subsequently, asphaltene aggregates can migrate to bottom-hole and to the near wellbore formation as reservoir depletion progress, altering the most important petrophysical properties of formation rock (i.e., porosity and permeability). However, in some petroleum fields, wellbore impairment has even started in early stages of production due to the precipitation and deposition of asphaltenes.[2,5,6,13,15,37]

Deposition of precipitated asphaltenes over pore surfaces and/or across pore throats may reduce the effective pore space and/or severely impair the ability of crude oil to flow through a porous formation. Therefore, asphaltene deposition can cause an important formation damage and, as a result, diminish the productivity in petroleum reservoirs during oil production;[1−3,6,9,11,12,25,38] thereby, the key to maintain a good productivity in wells is prevention of permeability damage, since having a clear understanding of the asphaltene deposition mechanism can help the oil industry to develop effective engineering practice to minimize asphaltene deposition in oil-bearing formations

(15) Minssieux, L.; Nabzar, L.; Chauveteau, G.; Longeron, D.; Bensalem, R. *Rev. Inst. Franç. Pet.* **1998**, *53* (3), 313–327.
(16) Shedid, S. A. *Pet. Sci. Technol.* **2001**, *19* (5&6), 503–519.
(17) Ghloum, E. F.; Oskui, G. P. *Pet. Sci. Technol.* **2004**, *22* (7&8), 1097–1117.
(18) Papadimitriou, N. I.; Romanos, G. E.; Charalambopoulou, G. Ch.; Kainourgiakis, M. E.; Katsaros, F. K.; Stubos, A. K. *J. Pet. Sci. Eng.* **2007**, *57*, 281–293.
(19) Hamadou, R.; Khodja, M.; Kartout, M.; Jada, A. *Fuel* **2007**, *87*, 2178–2185.
(20) Mirzayi, B.; Vafaie-Sefti, M.; Mousavi-Dehghani, S. A.; Fasih, M.; Mansoori, G. A. *Pet. Sci. Technol.* **2008**, *26*, 231–243.
(21) Hansen, P. W. A CO_2 tertiary recovery pilot. Little Creek field, Mississippi. In SPE 6747 presented at the SPE Annual Technical Conference and Exhibition, Denver, CO, October 9−12, 1977; p 1.
(22) Krueger, R. F. *Pet. Sci. Technol.* **1986**, 131–152.
(23) Jacobs, I. C.; Thorne, M. A. Asphaltene precipitation during acid stimulation treatments. In SPE 14823 presented at the Seventh SPE Symposium on Formation Damage Control of the Society of Petroleum Engineers held in Lafayette, LA, Febraury 26−27, 1986; p 131.
(24) Porter, K. E. *Pet. Sci. Technol.* **1989**, 780–786.
(25) Escobedo, J.; Mansoori, G. A. Heavy organic deposition and plugging of wells (Analysis of Mexico's experience). In SPE 23696 presented at the Second Latin American Petroleum Engineering Conference, II LAPEC, of the Society of Petroleum Engineers held in Caracas, Venezuela, March 8−11, 1992; p 349.
(26) Mansoori, G. A. *J. Pet. Sci. Eng.* **1997**, *17*, 101–111.
(27) Allenson, S. J.; Walsh, M. A. A novel way to treat asphaltene deposition problems found in oil production. In SPE 37286 presented at the SPE International Symposium on Oilfield Chemistry held in Houston, Texas, February 18−21, 1997; p 699.
(28) Monger, T. G.; Trujillo, D. E. Organic deposition during CO_2 and rich-gas flooding. In SPE 18063 presented at the SPE Annual Technical Conference and Exhibition held in Houston, October 2−5, 1991; p 17.
(29) de Pedroza, T. M.; Calderon, G.; Rico, A.*SPE 27069 Advanced Technology Series*, **1995**, *4* (1), 185.
(30) Ju, B.; Luan, Z.; Wu, Z.; Lu, G. A study of removal of organic formation damage by experiments and modeling approaches. In SPE 68752 presented at the SPE Asia Pacific Oil and Gas Conference and Exhibition held in Jakarta, Indonesia, April 17−18, 2001; p 1.
(31) Zekri, A. Y.; Shedid, S. A. *J. Pet. Sci. Eng.* **2004**, *42*, 171–182.
(32) Negahban, S.; Bahamaish, J. N. M.; Joshi, N.; Highswander, J.; Jamaluddin, A. K. M. An experimental study at an Abu Dhabi reservoir of asphaltene precipitation caused by gas injection. In SPE 80261 presented at the SPE International Symposium on Oilfield Chemistry, Houston, Texas, February 5−7, 2005; p 115.
(33) Sim, S. S. K.; Takabayashi, K.; Okatsu, K.; Fisher, D. Asphaltene-induced formation damage: effect of asphaltene particle size and core permeability. In SPE 95515 presented at the SPE Annual Technical Conference and Exhibition held in Dallas, Texas, U.S.A., October 9−12, 2005; p 1.
(34) Zekri, A. Y.; Shedid, S. A.; Alkashef, H. *J. Pet. Sci. Eng.* **2007**, *59*, 300–308.
(35) Hirschberg, A.; de Jong, L. N. J.; Schipper, B. A.; Meijer, J. G. *Soc. Pet. Eng. J.* **1984**, 283–293.
(36) Almehaideb, R. A. *J. Pet. Sci. Eng.* **2004**, *42*, 157–170.
(37) Galoppini, M.; Tambini, M. Asphaltene deposition monitoring and removal treatments: An experience in ultra deep wells. In SPE 27622 presented at European Production Operations Conference and Exhibition held in Aberdeen, U. K., March 15−17, 1994; p 253.
(38) Wang, S.; Civan, F. *J. Energy Resourc. Technol.* **2005**, *127*, 318–321.
(39) Garland, E. The asphaltic properties of an apparently ordinary crude oil may lead to re-thinking of field exploitation. In SPE 19731 presented at the 64th Annual Technical Conference and Exhibition of the Society of Petroleum Engineers held in San Antonio, Texas, October 8−11, 1989; p 281.
(40) Thawer, R.; Nicoll, D. C. A.; Dick, G. Asphaltene deposition in production facilities. In *SPE Production Engineering*; November, 1990; pp 475−480.
(41) Takhar, S. Prediction of asphaltene deposition during production-model description and experimental details. In SPE 30108 presented at the European Formation Damage Conference held in The Hague, The Netherlands, May 15−16, 1995; p 311.

and develop treatment programs to restore well productivity.[5,6,11,22]

1.1. Asphaltene Deposition vs Precipitation. The terms deposition or flocculation have often been used to describe the precipitation process. It is important to clarify the difference between the two. Although precipitation may be defined as the formation of a solid phase out of a liquid phase, deposition can be described as the formation of a layer of the precipitated solid on a surface. Further, a necessary but not a sufficient condition for deposition is the precipitation of a solid phase from liquid solution. That is, precipitation, although a precursor to deposition, does not necessarily cause deposition. Moreover, whereas the precipitation is mainly a function of thermodynamic variables such as composition, pressure, and temperature, the deposition is also dependent on the flow hydrodynamics and the surface-solid interactions. It is important not only to identify the factors that influence the deposition process but also to understand how they affect the process.

This work presents results of phase behavior of live crude oil and coreflood tests conducted at reservoir pressure and temperature conditions to identify the dominant factors associated with permeability reduction during primary oil recovery. Initially, the phase behavior of the reservoir fluid was measured to know the presence of asphaltenes. Then, laboratory coreflood tests were performed to investigate the effect of asphaltene deposition in reduction of core permeability. The asphaltene precipitation on porous medium was induced by diminished pressure as it occurs during the primary oil production. Investigated variables included pressure drop, flow rate, initial absolute permeability, and effective porosity. The porous medium used was Bedford limestone rock. The core tests were conducted at 413.9 K and at pressures between the upper boundary and bubble-point pressures. The network model proposed was used to predict formation damage due to in situ asphaltene deposition; this model was qualitatively evaluated using data from this work and those reported in the literature. Results are in concordance with expected physical behavior.

2. Experimental Section

2.1. Reservoir Fluid Sample and Core. The representative single-phase bottom-hole sample used in this work was collected from a Mexican reservoir (light crude oil from the Southeast region of Mexico), which has a serious asphaltene deposition problem during its primary production stage.[25,42] To simulate the oil-bearing formation, a consolidated Bedford limestone core having cylindrical shape (diameter 1.5 in., length 2 in.) was characterized and tested in laboratory.

2.2. The Bulk Apparatus. Reservoir temperature and pressure conditions of a single-phase bottom-hole sample were reproduced in laboratory in order to get the best possible and most representative sample[43] using a bulk apparatus. This apparatus has a rocking mechanism that imparts an oscillating motion to sample cylinders normally associated with reservoir fluids; the cylinders are oscillated through 60° about its center of gravity, at a rate of about 40 cycles per minute. The motion agitates the contained fluids in order to bring them to an equilibrium condition. The bulk cell is thermo-regulated by means of an airbath oven (Despatch, model Ecosphere EC-335, temperature range of 200.2−450.2 K) and the temperature is measured with a Pt-100 Ω/0 °C resistance thermometer (PRT), which is inserted inside a thermometric well of the stainless steel high-pressure cylinder.

2.3. The High Pressure Visual *PVT* Apparatus with Solid Detection System (SDS). To identify the onset of asphaltene precipitation as well as the bubble-point pressure curve of the reservoir fluid, a fully visual variable volume *PVT* apparatus (maximum working pressure of 103.4 MPa, maximum temperature of 473.2 K) equipped with a laser-based particle detection system was used. The operation principle of this technique applied to reservoir fluids, especially to the asphaltene problematic, has been described in detail elsewhere.[17,44−48] This *PVT* cell mainly consist of (i) a phase behavior cell, (ii) a glass cylinder, (iii) a high-pressure positive displacement pump, (iv) a temperature-controlled oven, (v) a resistance temperature detector, (vi) a digital pressure indicator, (vii) stainless steel high pressure cylinders equipped with floating pistons, (viii) a back pressure regulator, (ix) a magnetic mixer, (x) a data acquisition interface, (xi) a solid detection system, and (xii) a video-based level measurement system. Figure 1 shows the schematic diagram of the experimental setup used in this investigation to measure the asphaltene precipitation envelope (APE) upper boundary as well as the bubble-point pressure curve of the reservoir fluid. The SDS consists of a mercury-free, variable volume, fully visual *PVT* cell equipped with fiber optics light transmission probes (source and detection) to measure the onset of organic solids precipitation (due to temperature, pressure, and compositional change) concurrently with fluid volumetric data.[17,44]

2.3.1. Temperature Measurement and Regulation of the PVT Cell. The phase behavior cell is thermo-regulated by means of an airbath oven in the temperature range from 239 to 463 K. A Pt-100 Ω/0 °C resistance thermometer (PRT) is inserted inside a thermometric well of the *PVT* cell body. The PRT and the digital panel meter were calibrated with a platinum resistance thermometer (T100−450) with an overall uncertainty of ±0.1 °C in the working temperature range.

2.3.2. Pressure Measurement of the PVT cell. The DBR Series II high pressure positive displacement pump (maximum working pressure of 103.4 MPa, total volume of 150 mL, volume resolution as fine as 0.0025 mL, flow rate accuracy of ±0.02%) is used to transfer the fluid as well as to reach the desired pressure in the whole system. Pressures were measured by means of a transducer (Heise, model 901A, pressure range from 0 to 68.9 MPa) connected to the measurement circuit. The pressure transducer was calibrated against a dead weight balance (Pressurements, model M2200 A, accuracy of 0.015% in full scale). The estimated uncertainty of the pressure measurements is ±0.02% in the working pressure range.

2.4. Gasometer. To know the gas−oil ratio (GOR) of the reservoir fluid, a single-stage flash apparatus (capacity of 10 L, maximum flow rate of 40 L/h, volume resolution of 0.253 mL) was used. This apparatus uses a motor-driven piston in a stationary cylinder. The piston displacement is monitored to

(42) Barcenas, M.; Orea, P.; Buenrostro-Gonzalez, E.; Zamudio-Rivera, L. S.; Duda, Y. *Energy Fuels* **2008**, *22*, 1917–1922.

(43) Bon, J.; Sarma, H. K.; Rodriguez, J. T.; Bon, J. G. Reservoir fluid sampling revisited-A practical perspective. In SPE 101037 presented at the SPE Asia Pacific Oil & Gas Conference and Exhibition held in Adelaide, Australia, September 11−13, 2006; p 1.

(44) Hammami, A.; Phelps, C. H.; Monger-McClure, T.; Little, T. M. *Energy Fuels* **2000**, *14*, 14–18.

(45) Aquino-Olivos, M. A.; Buenrostro-Gonzalez, E.; Andersen, S. I.; Lira-Galeana, C. *Energy Fuels* **2001**, *15*, 236–240.

(46) Jamaluddin, A. K. M.; Creek, J.; Kabir, C. S.; McFadden, J. D.; D'Cruz, D. A comparison of various laboratory techniques to measure thermodynamics asphaltene instability. In SPE 72154 presented at the Asia Pacific Improved Oil Recovery Conference held in Kuala Lumpur, Malaysia, October 8−9, 2001; p 1.

(47) Jamaluddin, A. K. M.; Joshi, N.; Iwere, F.; Gurpinar, O. An investigation of asphaltene instability under nitrogen injection. In SPE 74393 presented at the SPE International Petroleum Conference and Exhibition in Mexico held in Villahermosa, Mexico, February 10−12, 2002; p 1.

(48) Aquino-Olivos, M. A.; Andersen, S. I.; Lira-Galeana, C. *Pet. Sci. Technol.* **2003**, *21* (5&6), 1017–1041.

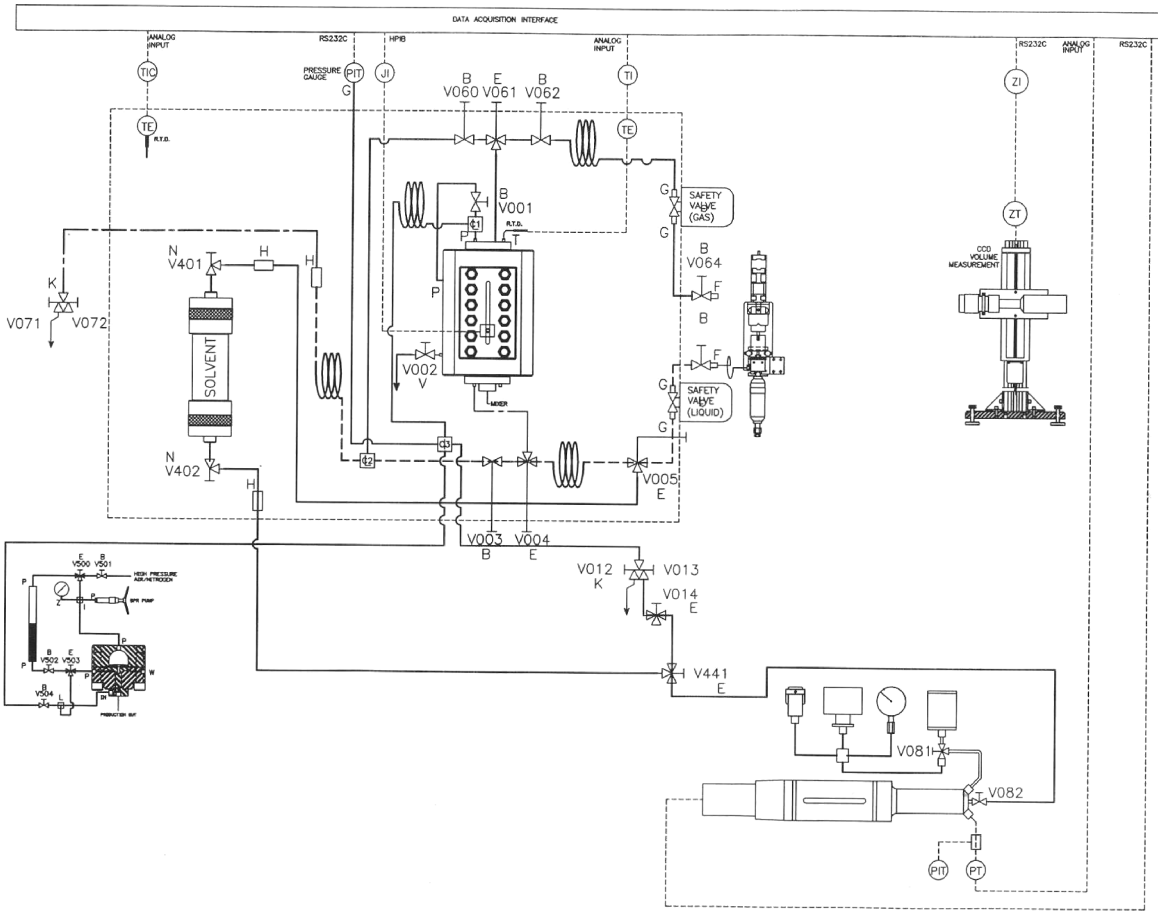

Figure 1. Schematic diagram of phase behavior system of reservoir fluid for mercury-free operation.

determine the swept volume of the cylinder. The cylinder pressure is automatically held at atmospheric pressure. As gas enters to the gasometer, a pressure sensing device responds to any pressure change and instructs a motor to reposition the piston. This restores a null pressure reading in the gasometer. Piston motion is tracked by a linear encoder. This reading is converted to show the gas volume in the cylinder.

The gasometer uses a pressure transducer to measure the absolute pressure in the gasometer cylinder. The pressure transducer output is fed to a digital voltmeter that controls the piston drive motor to maintain the set pressure. A thermocouple was inserted inside the cylinder bottom to measure the ambient temperature. Two stainless steel pycnometers (capacity of 75 mL, maximum working pressure of 12.4 MPa) were connected to the entire arrangement of the gasometer; one of them contains the reservoir fluid while the second one contains the released gas during the expansion process.

2.5. Gas and Liquid Chromatography. When the reservoir fluid sample was flashed at atmospheric conditions, vapor and liquid phases were analyzed by means of the high temperature gas chromatography (HTGC) technique. To analyze the lighter fraction up to C_{15+} (including CO_2, H_2S, and N_2) a high temperature gas chromatograph (HP, model 6890) (three packed columns and one capillary column) with thermal conductivity and flame ionization detectors is used while the residual liquid was analyzed up to C_{30+} with another high temperature gas chromatograph (HP, model 6890) (a capillary column) that includes a flame ionization detector. From the measured composition, total mass of each phase, and the GOR, the composition of the original reservoir fluid was calculated by mass balance.

For SARA (saturates, aromatics, resins, and asphaltene) fraction analysis, asphaltene fraction was extracted from dead crude oil (residual oil) by precipitation with n-heptane as described by the ASTM D3279−97 procedure. The maltene fraction was separated in saturates, aromatics, and resins using ASTM D891−95 procedure by high performance liquid chromatography (HPLC) technique as it has been described elsewhere[49] using an amino-modified silica column with n-heptane, dichloromethane, and chloroform as elution solvents.

2.6. High Pressure Viscometer. To determine the viscosity behavior of the reservoir fluid, at the study temperature and different pressures, a constant force electromagnetic viscometer (Cambridge Applied Systems Inc., SPL440 model, maximum working pressure of 137.9 MPa, maximum temperature of 463.2 K) was used.

2.7. Coreflooding System. Figure 2 shows the schematic diagram of the experimental setup used in this work in order to determine the effect of asphaltene-induced precipitation and deposition on the petrophysical properties of a reservoir rock. This setup consists mainly of the following devices: (i) two dual positive displacement computerized pumps, (ii) high pressure stainless steel cylinders equipped with floating pistons (capacity of 500 mL, maximum working pressure of 68.9 MPa), (iii) a core holder (maximum working pressure of 75.8 MPa at a maximum temperature of 422.0 K), (iv) a visual stainless steel cell, (v) a pressure transducer (DPI, Paroscientific, model 410K-HHT-101, pressure range from 0 to 68.9 MPa), (vi) a back-pressure regulator, (vii) an overburden pump, (viii) an air-bath oven, (ix) rigid valves, (x) a data acquisition system (pressure, temperature, volume), and (xi) a fractional collector.

2.7.1. Core Holder. The core holder, horizontally placed, holds a core through a Viton sleeve with a size of 1.5 in. diameter

(49) Buenrostro-Gonzalez, E.; Espinosa-Peña, M.; Andersen, S. I.; Lira-Galeana, C. *Pet. Sci. Technol.* **2001**, *19* (3&4), 299–316.

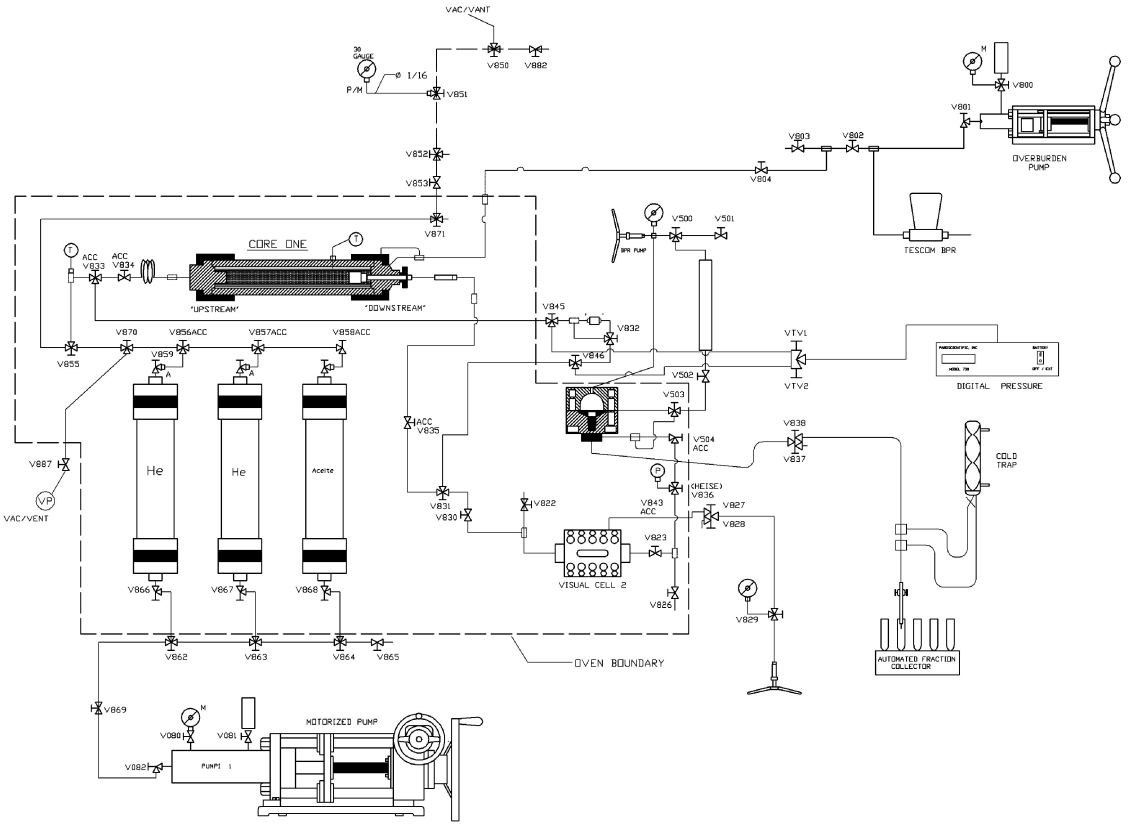

Figure 2. Schematic diagram of the experimental setup to carry out displacement test in porous media.

and 15.69 in. overall length. A constant overburden pressure was applied around this sleeve by connecting it to a nitrogen/water bottle, which maintained a constant overburden pressure of 3.4 MPa around the sleeve. The core holder has three inlet ports, and one outlet port for fluid production.

The inlet and outlet ports of the core holder are connected to the pressure transducer. The inlets ports of the core holder are also connected to the positive displacement pump (PDP). One cylinder containing the single-phase fluid sample allowed injection of sample inside the core holder. The PDP was operated in constant rate mode and with an accuracy of 0.06 mL/h. The outlet port of the core holder was connected to the fractional collector through a back pressure regulator for collection of produced fluids from the core.

2.7.2. Temperature and Pressure Measured in the Core Holder. The pressure drop during the coreflood tests was measured with a digital pressure indicator (DPI); the DPI was calibrated against a dead weight balance with an uncertainty in pressure of ±0.01% in full scale. The coreflooding system was thermoregulated by means of an airbath oven (maximum operating temperature of 423.2 K, uniform airbath temperature distribution of ±1 °C, set-point temperature resolution of ±0.1 °C), which is a precision built, electrically heated, temperature-controlled forced-air. A Pt-100 Ω/0 °C resistance thermometer (PRT) was inserted inside a thermometric well of the core holder. The PRT was calibrated with a platinum resistance thermometer (T100−450) with an overall uncertainty of ±0.1 °C in the working temperature range.

2.8. Experimental Procedure. The evaluation of the formation damage (core permeability reduction) was carried out in the following sequences:

Characterization of the Reservoir Fluid Sample: (1) Re-establish the reservoir conditions of the single-phase bottom-hole sample by means of the bulk apparatus. (2) Determine the asphaltene precipitation envelope (APE) upper boundary and bubble-point pressure curve (at least at four temperature points, including reservoir temperature) using the high pressure *PVT* apparatus. (3) Determine the original compositional analysis of the reservoir fluid sample by means of the HTGC technique. (4) Determine the SARA analysis of the dead crude oil using HPLC technique. (5) Measure the dynamic viscosity of the fluid sample at the study temperature and different pressures.

Characterization of the rock-fluid system: (1) Measure the initial effective porosity of the core. (2) Determine the liquid or absolute permeability using Darcy's law (the Klinkenberg effect, i.e., variation in gas permeability with mean pressure and type of gas). (3) Set the study temperature for the core test. (4) Inject the live crude oil to saturate the core at the temperature and pressure chosen (based on the APE upper boundary and bubble-point pressure curve). (5) Inject several pore volumes of live crude oil at a constant flow rate. (6) Measure the pressure drop along the core and calculate the absolute permeability using Darcy's law (reference liquid permeability, k_i). (7) Decrease pressure to a slightly higher pressure than that of bubble-point pressure. (8) Displace several pore volumes of live crude oil and measure the damaged permeability, k_d, under similar conditions of temperature and flow rate used for measuring k_i. (9) Flush the core with cyclohexane at the same conditions for measuring k_d to measure the final absolute permeability, k_f (damage due to asphaltene deposition). (10) Measure the final effective porosity, ϕ_f.

2.8.1. Reservoir Fluid Sample and Preparation. At the laboratory, the reservoir fluid was isothermally and isobarically charged from the storage cylinder (proprietary single-phase sampling technology) to a high-pressure stainless steel cylinder (capacity of 1 L and a maximum working pressure of 68.9 MPa) using a PDP (capacity of 1 L and a maximum working pressure of 68.9 MPa). Reservoir temperature and pressure conditions of the fluid sample were reconditioned using the bulk apparatus. The representative sample of the reservoir fluid was maintained with agitation during a week to ensure it was at a single-phase

condition. The high-pressure cylinder containing the reservoir fluid was placed in an air-bath oven (integral part of the bulk apparatus) where it was equilibrated at the temperature of 428.2 K and a pressure of 55.2 MPa. The fluid pressure was controlled by means of the PDP during the reconditioning process. The cylinder containing the fluid sample was placed under intermittent rocking for a week. Subsequently, aliquots of the equilibrated fluid were displaced (at isothermally and isobarically conditions) inside the visual *PVT* cell in order to carry out a constant composition experiment (CCE).

2.8.2. APE Upper Boundary and Saturation Curve. Initially, the visual *PVT* cell was completely cleaned up (including its peripheries that form the measuring circuit, see Figure 1) and evacuated (until system reached an appropriate vacuum) at the reservoir temperature. A sample volume of 30−50 mL was isothermally and isobarically (at reservoir pressure) transferred to the fully visual *PVT* cell from the cylinder containing the reservoir fluid (after it was reconditioned). The sample volume was used to carry out the CCE in order to measure one point (upper boundary of the p-T diagram) of the APE as well as one point of the fluid bubble-point pressure corresponding to that temperature. When reservoir temperature and pressure were equilibrated, the software for monitoring the CCE was activated and the parameters to control the experiment (flow rate of 10 mL/h, *PVT* data record each 10 s) were set. At the time that the experiment was started (to a constant power transmittance light), the pressure of the system was diminished isothermally at a programmable rate (from reservoir pressure to approximately 3.4 MPa) maintaining the agitation continuously into the cell. The experiment was stopped until the programmable pressure was reached.

When the CCE was stopped, the *PVT* cell was cleaned up and evacuated. Afterward, a new load of sample volume was transferred into the *PVT* cell and the process of depressurization (CCE) of the sample fluid until at and by below the bubble-point pressure was repeated at temperatures of 387.2, 345.2, and 303.2 K to build a reliable complete *P*−*T* diagram for the onset of asphaltene formation and from that, select the temperature and pressure conditions to carry out the core test experiments.

2.8.3. Gas−Oil Ratio. When the reservoir fluid was reconditioned, an aliquot of known volume (10−12 mL) was withdrawn isothermally and isobarically into an evacuated and preweighed pycnometer to determine the original compositional analysis of the reservoir fluid. The pycnometer containing the fluid sample was then connected to the DBR gasometer where the fluid was flashed to atmospheric pressure condition to know the gas volume released and the amount of residual liquid. Next, the evolved gas phase was circulated through the residual liquid for a period of time to achieve equilibrium between phases. The vapor phase was collected in a second pycnometer (previously connected to the gasometer) of the same features (capacity of 75 mL and a maximum working pressure of 12.4 MPa). Once equilibrium was achieved, the volume of vapor and the mass of liquid remaining in the pycnometer were measured to calculate the GOR.

2.8.4. Compositional and SARA Analysis. The pycnometer containing the vapor phase, after the single stage flash test, was connected to a circuit through the inlet of the high temperature gas chromatograph (with integrated thermal conductivity and flame ionization detectors) to analyze the lighter fraction (CO_2, H_2S, N_2, C_1−C_{15+}) of crude oil. An aliquot was withdrawn from the pycnometer containing the residual liquid (dead crude oil) to analyze the heavy fraction up to C_{30+} using a second high temperature gas chromatograph with an integrated flame ionization detector. From the measured composition by both chromatographs, total mass of each phase, and the GOR, the composition of the original reservoir fluid was calculated by mass balance. For SARA fraction analysis, asphaltene fraction was extracted from dead crude oil (residual oil) by precipitation with n-heptane as described by the ASTM D3279−97 procedure. The maltene fraction was separated in saturates, aromatics, and resins using ASTM D891−95 procedure by an HPLC technique as it has been described elsewhere.[49]

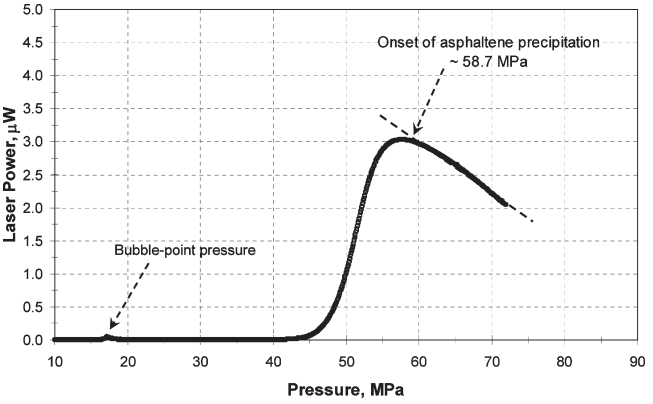

Figure 3. Behavior of PTL as a function of the pressure depletion process at a constant temperature.

2.8.5. Viscosity Isotherm. An aliquot of known volume (15−20 mL) was taken out, at study conditions, from the high-pressure stainless steel cylinder containing the single-phase bottom-hole sample in order to know the viscosity behavior of the reservoir fluid as a function of pressure at the study temperature of 413.9 K. First, the fluid sample was isothermally and isobarically transferred to a high pressure cylinder (capacity of 250 mL and a maximum working pressure of 68.9 MPa). Afterward, the sample was loaded to the electromagnetic viscosimeter at isothermal and isobaric conditions. The viscosity changes at different pressures were measured, and the bubble-point pressure was determined by this technique too.

2.8.6. Core Preparation, Initial Effective Porosity, and Equivalent Gas Permeability. The consolidated Bedford limestone core was cleaned before its use with toluene using the Soxhlet extraction for 24 h. Afterward, it was dried in an oven with vacuum system at 373 K during 24 h and cooled in a desiccator. Then, the core was tested in the laboratory in order to measure the initial effective porosity, as well as the equivalent gas (helium) permeability at a specified mean pressure (6.9 MPa) using a core measurement system (CMS-300, model 300).

Once these initial parameters were measured as a reference, the core was mounted along with sleeve into the core holder. After that, all pipelines were connected to the coreflooding system (Figure 2); then, the study temperature was set and the whole system was evacuated during all night. As a first dynamic experiment, the initial effective porosity was measured at one confining pressure of 6.9 MPa in order to reproduce the value obtained with the CMS-300, as well as to determine the equivalent gas permeability at the same confining pressure.

3. Results and Discussion

3.1. Phase Behavior of Reservoir Fluid. Figure 3 shows a typical plot of the power of transmitted light (PTL) versus pressure measured for a live crude oil, at a constant temperature (reservoir temperature of 428.2 K). PTL is the amount of light that passes through the crude oil sample inside a visual *PVT* cell and recorded by the receiving fiber optic cable.[17,44] As the fluid pressure was diminished, asphaltenes begin to agglomerate and block the path of the laser signal being transmitted through the fluid inside the cell. Such behavior was observed in Figure 3 as a sharp drop in PTL. From Figure 3 also it was possible to determine the bubble-point pressure by changing the scale of the graph and analyzing its behavior as pressure diminish by below the onset of asphaltene precipitation. This value of

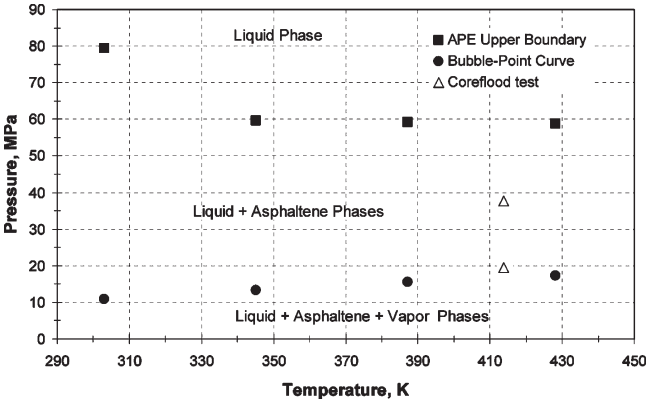

Figure 4. $P-T$ diagram of the reservoir fluid. The triangle symbols show the reservoir pressure and temperature conditions where coreflood tests were carried out.

the bubble-point pressure is in good agreement with the conventionally measured value ($P-V$ plot) in Figure 4. By this light-scattering technique, the formation onset of asphaltene precipitation and the bubble-point pressure correspond to the points where the PTL value undergoes a slope change and a noticeable drop, respectively, as pressure of the system decreased. Composition expansion experiments were carried out at four temperatures. Figure 4 shows the $P-T$ diagram, at four temperatures, of the reservoir fluid used in the investigation. As shown in Figure 4, the APE upper boundary is consistent with the trend typically observed and reported from CEE using the PVT cell (equipped with a laser-based particle detection system) for crude oils with asphaltene content.[50] The bubble-point pressure values were determined by means of the conventional $P-V$ technique.

3.2. Composition of the Sample. Table 1 shows the composition of the original reservoir fluid along with the molecular weight value obtained by means of gas chromatography technique, as well as the GOR value determined by the single-stage flash apparatus. The asphaltene content of the dead crude oil was 2.86 wt %, which was obtained by precipitation with n-heptane following the ASTM D3279−97 procedure. Table 2 shows the SARA analysis of the crude oil obtained by the HPLC technique. The °API (29.3) of the dead crude oil was determined at a temperature of 298.2 K, following the ASTM D891−95 procedure. From the °API value, the crude oil can be considered as a medium crude oil.

3.3. Viscosity Isotherm at Study Temperature and Different Pressures. Figure 5 shows the viscosity behavior of the reservoir fluid from reservoir pressure to bubble-point pressure (at the temperature of 414.0 K) of the live crude oil sample. Points A and B on the graph correspond to the points (μ vs p) where core tests were carried out. The bubble-point pressure measured by the electromagnetic viscometer was of 17.0 MPa, finding a maximum difference of 1.6% in comparison to that found with the conventional P-V technique.

3.4. Coreflood Tests with Live Crude Oil Sample. As a first dynamic experiment, the initial effective porosity was measured at one confining pressure of 6.9 MPa in order to reproduce the value obtained with the CMS-300, as well as to determine the equivalent gas permeability at the same confining pressure. The consistency between porosity measurement carried out by means of the experimental arrangement described previously and that obtained by the CMS-300 were analyzed, finding a maximum difference of 1.2%. The effective porosity and equivalent gas permeability were also measured at the confining pressures of 20.7 and 34.5 MPa. Table 3 shows the porosity behavior when a confining pressure was applied to the core, at the average temperature of 293.5 K.

The equivalent gas permeability was measured at an average confining pressure of 7.4 MPa, at different constant flow rates, and an ambient temperature of 291.5 K (see Table 4); from these values, average equivalent gas permeability of 21.7 mD was obtained.

Table 1. Original Composition and Some Physical Properties of the Reservoir Fluid

	global	
component	wt %	mol %
CO_2	0.49	1.20
H_2S	0.04	0.12
N_2	0.18	0.70
C_1	5.01	34.05
C_2	3.09	11.21
C_3	2.87	7.10
i-C_4	0.52	0.98
n-C_4	1.69	3.17
i-C_5	0.91	1.38
n-C_5	1.41	2.13
C_6	2.94	3.82
C_7	3.48	3.50
C_8	3.75	3.67
C_9	3.22	2.74
C_{10}	3.74	3.04
C_{11}	3.25	2.41
C_{12}	2.72	1.84
C_{13}	2.56	1.59
C_{14}	2.32	1.33
C_{15+}	55.80	14.01
molecular weight	109	g/mol
GOR @ STD	121	m^3/m^3

Table 2. SARA Analysis of the Dead Crude Oil Sample (Reservoir Fluid Sample after Pressure Depletion)

group	wt %
saturates	44.65
aromatics	34.55
resins	17.90
asphaltenes	2.86

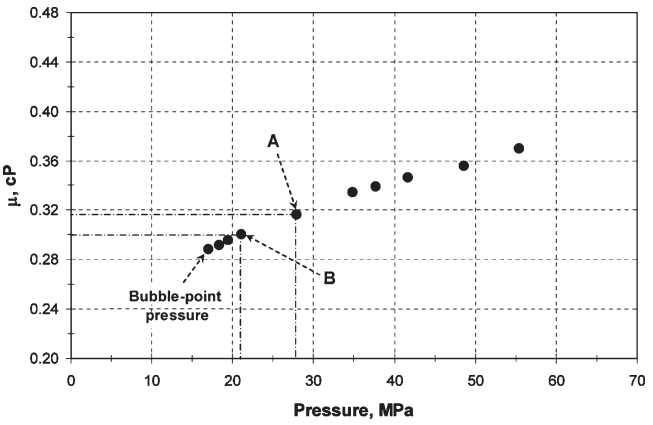

Figure 5. Viscosity isotherm of the live crude oil at study temperature from reservoir pressure to bubble-point pressure.

(50) Leontaritis, K. J. *Fuel Sci. Technol. Int.* **1996**, *14* (1&2), 13–39.

Table 3. Porosity Variation with the Confining Pressure Applied to the Core (at 293.5 K)

confining pressure (MPa)	effective porosity (%)
6.9	15.4
20.7	11.8
34.5	10.4

Table 4. Equivalent Gas Permeability at 7.4 MPa and at Different Flow Rates

T (K)	flow rate (mL/h)	equivalente gas permeability (mD)
291.6	499.68	22.6
291.5	1000.08	22.3
291.5	1500.12	21.2
291.2	1999.80	20.9

Table 5. Equivalent Gas Permeability at Different Confining Pressures (At Ambient Temperature)

confining pressure (MPa)	equivalent gas permeability (mD)
7.4	21.6
21.4	19.9
36.1	19.1

Similarly, equivalent gas permeabilities were measured at the confining pressures of 21.4 and 36.1 MPa and at ambient temperature (see Table 5). During all these and subsequent experiments, a constant overburden pressure of 3.4 MPa was maintained around the sleeve.

From the experimental data of Table 5, it was possible to determine the equivalent liquid permeability by plotting the reciprocal of the average confining pressure of the test and the equivalent gas permeability. The line fitted when extrapolated to infinite average pressure intercepts the permeability axis, at which point it is designated as the equivalent liquid permeability. According to this, the value found was of 18.7 mD. The equivalent gas permeability measured with the CMS-300 was of 24.0 mD, finding a maximum difference of 28.5%. However, it is well-known that permeability of gas depends on factors that influence the mean free path, such as temperature, pressure, and the molecular size of the gas. At high confining pressure, it is important to mention that equivalent gas permeability is close to that of 18.7 mD; therefore, we considered this value as the initial absolute permeability of the core.

3.4.1. Core Damage During Pressure Depletion at a Point Inside APE. Dynamic flow experiments were carried out at a study temperature of 413.9 K using a live crude oil and a Bedford limestone core sample inserted into the experimental model, shown in Figure 2. The core and pipelines of the coreflooding system were evacuated all a night. Afterward, the core was saturated with the crude oil and brought to a confining pressure inside the APE (see Figure 4, higher triangle symbol that corresponds to the point A in Figure 5). The chosen pressure to carry out the core test was 37.7 MPa, where the process of asphaltene precipitation had already occurred. When the study temperature and pressure were stabilized, live crude oil was injected to the core at a constant flow rate of 10 mL/h. At this flow rate, it was injected at least 10 pore volumes of crude oil; no plugging was detected, and a stable oil permeability was achieved (Figure 6a). Then, the flow rate was increased to 20 mL/h, and approximately 25 pore volumes were injected to the core; no alteration on oil permeability was observed (Figure 6b). Finally, the flow rate was increased to 40 mL/h, and oil permeability was monitored. At least 42 total pore volumes were injected to the core and no plugging was noted (Figure 6c); oil permeability remained stable throughout the injection of crude oil. Figure 6 shows oil permeability versus throughput results. The average oil permeability was calculated to be 18.5 mD for the three constant flow rates. This oil permeability value found, at these conditions, is very similar to that value determined from equivalent gas permeability (18.7 mD); the maximum difference was of 0.9%.

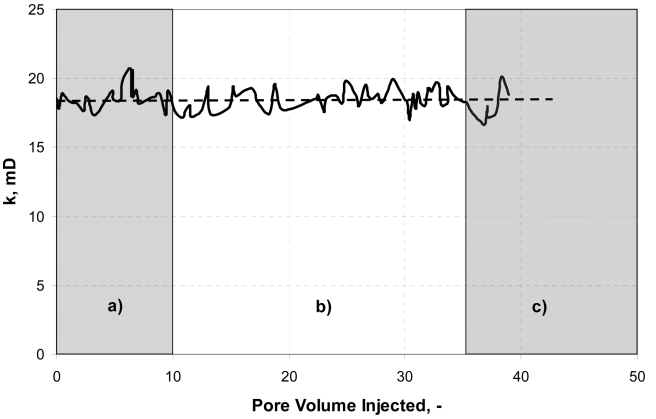

Figure 6. Oil permeability versus throughput (414.0 K and 37.7 MPa); (a) 10, (b) 20, and (c) 40 mL/h.

3.4.2. Core Damage during Pressure Depletion at a Point Near Bubble-Point Pressure. After several pore volumes of injected live crude oil where no plugging was noted, the fluid pressure into the coreflooding system was slowly decreased until a pressure of 19.5 MPa was reached; as it can be seen in Figure 4 (lower triangle symbol that corresponds to the point B in Figure 5), this pressure is slightly above the bubble-point pressure (see Figures 4 and 5). Field experiences have demonstrated that the asphaltene precipitation and deposition problems are much more severe when the reservoir fluid pressure is at the bubble-point than when the pressure is below the bubble-point.[2,12] Due to this pressure condition and that reported in the literature,[13,15,40,51−53] the presence of larger asphaltene aggregates may obstruct the fluid flow though the core. When confining pressure was stabilized in the system, a constant flow rate of 40 mL/h was set, and several pore volumes were injected to the core. The pressure drop was then measured, and the oil permeability was monitored. After 10 pore volumes injected (Figure 7), it was noted that oil permeability behavior was slightly changed. When 15 pore volumes were injected, the oil permeability decreased gradually, as can see from Figure 7. At least 35 pore volumes were injected through the full core, and the oil permeability behavior was monitored. Due to the limiting of live crude oil volume, it was not possible to inject more oil into the core. From results shown in Figure 7, it was possible to note that core permeability damage increases continuously as the pore volume of injected crude oil increases. At the end of nearly 34 pore volumes of crude oil throughput,

(51) Burke, N. E.; Hobbs, R. E.; Kashou, S. F. *JPT* **1990**, 1440–1446.
(52) Ellison, B. T.; Gallagher, C. T.; Lorimer, S. E. The physical chemistry of wax, hydrates, and asphaltenes. In OTC 11963 presented at the Offshore Technology Conference held in Houston, Texas, May 1−4, 2000; p 1.
(53) de Boer, R. B.; Leerlooyer, K.; Eigner, M. R. P.; van Bergen, A. R. D. Screening of crude oils for asphalt precipitation: Theory, practice, and the selection of inhibitors. In SPE 24987 first presented at the 1992 SPE European Petroleum Conference held in Cannes, November 16−18, 1995; p 55.

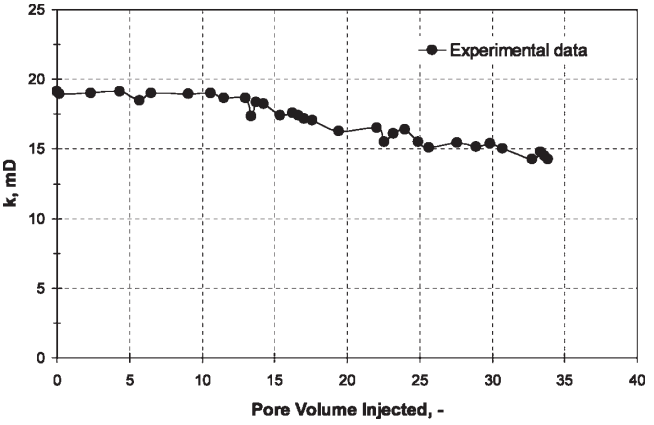

Figure 7. Oil permeability versus throughput at a confining pressure near bubble-point pressure and a constant flow rate of 10 mL/h.

Table 6. Equivalent Gas Permeability after Precipitation and Deposition Process (At Ambient Temperature)

confining pressure (MPa)	equivalent gas permeability (mD)
8.0	11.6
21.7	10.4
36.8	10.1

the calculated oil permeability across the full core reduced to 14.1 mD, corresponding to 24% of the initial oil permeability.

To measure the effective porosity after experiments of oil flow with asphaltene content through the core, nitrogen and cyclohexane were injected to the core in order to remove the residual crude oil. Cyclohexane was injected continuously at a constant flow rate; finally, the core was soaked with air for about a day in order to remove the solvent.

After the cleaning process of the core at the study temperature, the system temperature was carried out to ambient temperature. Then, the final effective porosity and equivalent gas permeability were measured; the final effective porosity was measured at a confining pressure of 6.9 MPa to be 12.3%, finding that asphaltene deposition caused a 20% loss of initial effective porosity. The equivalent gas permeability was calculated at different constant flow rates and different confining pressures. Table 6 shows the equivalent gas permeability values found after the precipitation and deposition process. From the experimental data in Table 6, the equivalent liquid permeability was calculated to be 9.7 mD (48% loss of initial liquid permeability); as can be noticed, this value is smaller than that measured with the live crude oil. This increment of permeability damage may be caused by the injection of cyclohexane to the core, thereby generating extra deposition of asphaltenes.

When displacement experiments were concluded and the consolidated core was removed from the core holder, it was possible to observe that the extent of precipitated asphaltene deposition was not uniform along the whole core, finding that larger asphaltene concentration was observed on the front face of the core; such behavior of nonuniform asphaltene deposition through porous media has already been reported in the literature.[18,54]

(54) Papadimitriou, N. I.; Romanos, G. E., Stubos, A. K., Steriotis, Th. A., Chatzichristos, C., Aurdal, T., Experimental investigation of asphaltene precipitation during oil-solvent flow in core samples, 13th European Symposium on Improved Oil Recovery, 2005, Budapest, Hungary, April 25−27.

3.5. Proposed Mathematical Models. Formation damage in petroleum reservoirs occurs as a consequence of the combined effects of many complex phenomena. Most of the formation damage models consider a single phase, and the dominant formation damage mechanisms are assumed to be the mobilization, fine migration, and retention of fine particles in porous matrix.[55] Particularly, the models for asphaltene deposition in core tests proposed by Ali and Islam[14] and Wang and Civan[56] include a mass balance equation that involves adsorption and trapping rate of asphaltenes on porous media, where two processes occurring simultaneously. On the other hand, Minssieux[13] suggests that both mechanisms occur at different times, that is, first a gradual reduction of the average porous size due to asphaltene adsorption and after a trapping due to the comparable size between the asphaltene particles and the average radii of pore throats. Before asphaltene plugging process develops, the initial step presumably lies in a fast adsorption of asphaltenes onto active sites of rock surface; subsequent thicker molecular structures (i.e., multilayers) seem to form, as indicated by the absence of a clear plateau in asphaltene adsorption isotherms on various dry mineral surfaces.[57−62] It then follows a slower more-or-less reversible hydrodynamic aggregation of asphaltene molecules suspended in the crude oil, possibly forming large enough aggregates so as to be retained at pore throats.

On the basis of the models of Khilar and Fogler[63] and Sharma and Yortsos,[64] in this work we represent the porous medium as a network of pore bodies (sites) connected by pore throats (bonds) (Figure 8), in which pore throats are assumed to occupy negligible volume compared to the volume of the pore bodies; thus, the contribution of pore throat volume is not significant to the total porosity of the medium. In this work, permeability reduction is assumed to occur due to the following two main mechanisms: (1) asphaltene particles of size significantly smaller than a given pore size deposit uniformly over pore bodies and pore throats, thus causing a gradual reduction of the pore throat radii; and (2) asphaltene particles larger in size than a given

(55) Civan, F. Evaluation and comparison of the formation damage models. In SPE 23787 presented at the International Symposium on Formation Damage Control held in Lafayette, Louisiana, February 25−27, 1992; p 219.

(56) Wang, S.; Civan, F. Productivity decline of vertical and horizontal wells by asphaltene deposition in petroleum reservoirs. In SPE 64991 presented at the SPE International Symposium on Oilfield Chemistry held in Houston, Texas, February 13−16, 2001; p 1.

(57) Dubey, S. T.; Waxman, M. H. Asphaltene adsorption and desorption from mineral surfaces. In SPE 18462 presented at the SPE Intl. Symposium on Oilfield Chemistry held in Houston, February 6−10, 1989; p 389.

(58) Piro, G.; Canonico, L. B.; Galbariggi, G; Bertero, L.; Carniani, C. Asphaltene adsorption onto formation rock: An approach to asphaltene formation damage prevention. In SPE30109 presented at the SPE European Formation Damage Conference held in The Hague, The Netherlands, May 15−16, 1995; p 156.

(59) Acevedo, S.; Ranaudo, M. A.; Escobar, G.; Gutiérrez, L.; Ortega, P. *Fuel* **1995**, *74*, 595–598.

(60) Acevedo, S.; Castillo, J.; Fernández, A.; Goncalvez, S.; Ranaudo, M. *Energy Fuels* **1998**, 386–390.

(61) Marczewski, A. W.; Szymula, M. *Colloids Surf., A* **2002**, *208*, 259–266.

(62) Mendoza de la Cruz, J. L.; Castellanos-Ramírez, I. V.; Ortiz-Tapia, A.; Buenrostro-González, E.; Durán-Valencia, C. de los Á.; López-Ramírez, S. *Colloids Surf., A* **2009**, *340*, 149–154.

(63) Khilar, K. C.; Fogler, H. S. Water sensitivity of sandstones. In *SPE (10103) J.*, **1983**, 55.

(64) Sharma, M. M.; Yortsos, Y. C. *AIChE J.* **1987**, *33* (10), 1636–1643.

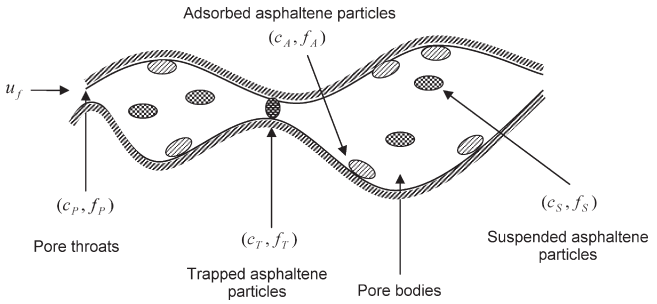

Figure 8. Rock−fluid system and elements of interest (taken from Khilar and Fogler[61]).

pore throat size are trapped by the pore throat, thus reducing the area allowed for fluid flow.[64]

Similarly as Khilar and Fogler[63] and Sharma and Yortsos,[64] the essential components to be considered in these models are: (a) suspended asphaltene particles, (b) adsorbed asphaltene particles, (c) trapped asphaltene particles, and (d) pore throats. Each group of particles is characterized by a volumetric concentration c_i and a particle size distribution f_i, and the pore throats are characterized by a volumetric concentration N_p and a pore throat size distribution f_p (see Figure 8).

To describe the permeability reduction caused by the asphaltene deposition in a porous medium, we propose two single models for adsorption and trapping of asphaltene considering that these two processes do not occur simultaneously; that is, adsorption first, followed by trapping. In this work, the asphaltene particles are considered as solid particles suspended in the crude oil. Thus, the precipitated asphaltene can deposit onto the rock surface through an adsorption process, or flow as suspended solid in the oil phase.[65]

3.5.1. Process of Asphaltenes Adsorption. When the diameter of the asphaltene particles is much smaller than the diameter of the pore throats, the trapping process is not considered as the origin in permeability reduction; however, permeability reduction is observed in such cases, even though it is a slower process. In this case, asphaltene adsorption process on the pore surface is considered as the major influence in the permeability change. Sharma and Yortsos[64] showed that the dimensionless material balance equations in the case of particles that are adsorbed on the pore walls (single pore size distribution) can be written as:

$$\frac{\partial c_{sD}(x_D, t_D)}{\partial t_D} + \frac{\partial c_{sD}(x_D, t_D)}{\partial x_D} = -\lambda c_{sD}(x_D, t_D) \quad (1)$$

$$\frac{\partial}{\partial t_D}(N_{pD} f_{pD}) = c_0 N_{pD} c_{sD}(x_D, t_D) \frac{\partial}{\partial r_{pD}}\left[f_{pD}\left(\frac{u_{RD}}{r_{pD}}\right)^{1/3}\right] \quad (2)$$

where the "D" subscript indicates that the variables are dimensionless; λ is a coefficient, and c_0 is a constant; c_{sD} is asphaltene concentration (number of particles per volume unit); N_{pD} is the number of pores per volume unit; f_{pD} is the pore throat size distribution; u_R is the interstitial velocity; r_{pD} is the pore radius; x is the length of the porous medium, and t is time.

(65) Nghiem, L. X.; Coombe, D. A.; Farouq-Ali, S. M. Compositional simulation of asphaltene deposition and plugging. In SPE Annual Technical Conference and Exhibition held in New Orleans, Louisiana, September 27−30, 1998; p 129.

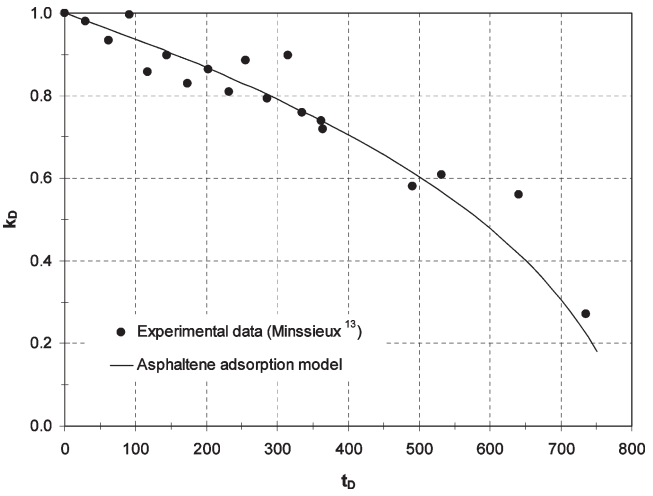

Figure 9. Comparison between experimental results obtained by Minssieux[13] (Run HMD 26) and those generated with asphaltene adsorption model developed in this work. $C_0 = 0.00125$ and $\lambda = 4$.

To find a solution to eq 2, we first need to solve eq 1 considering the following initial (eq 3) and boundary (eq 4) conditions:

$$c_{sD}(x_D, t_D = 0) = 0 \quad (3)$$

$$c_{sD}(x_D = 0, t_D) = 1 \quad (4)$$

To differ from Sharma and Yortsos,[64] we considered a unimodal pore size distribution of the form:

$$f_{pD} = \delta(r_{pD} - r^*_{pD}) \quad (5)$$

Considering an average asphaltene particle radii (r^*_p), it was possible to demonstrate (see Appendix) that permeability reduction due to asphaltene adsorption process can be predicted with the following expression:

$$k_D(t_D) = \frac{1}{\int_0^1 [(dx_D)/[1 - C_0 e^{-\lambda x_D}(t_D - x_D)]^2]} \quad (6)$$

where C_0 is an adjustable parameter. To validate our asphaltene adsorption model, eq 6 was applied to the experimental data (permeability reduction vs pore volume) reported by Minssieux[13] and compared to those generated by the adsorption model. From Figures 9 and 10, it is possible to observe that the proposed model fitted in good agreement with experimental data obtained by Minssieux.[13] C_0 and λ were adjusted to a value of 0.00125 and 4, respectively, for the experimental data in Figure 9. In this core test, Minssieux[13] used a dead crude oil with a low asphaltene content (0.15 wt %), viscosity of 1.5 at 80 °C, 43°API, and it was displaced with a injection rate of 8 mL/h. The porous medium selected for the flow test was a HMD core sample as an example of reservoir rock with an initial effective porosity of 7.1% and an initial permeability of 0.67 mD. This reservoir rock contains kaolinite as the main clay mineral. In this type of rock, permeability reduction started with an important adsorption of asphaltenes onto high specific area clays; then, it was followed by a hydrodynamic retention of asphaltene aggregates at pore throats, as it can seen in Figure 9.

For the case of the experimental data reported by Minssieux[13] on RUN GF1 core tests, the dead crude oil

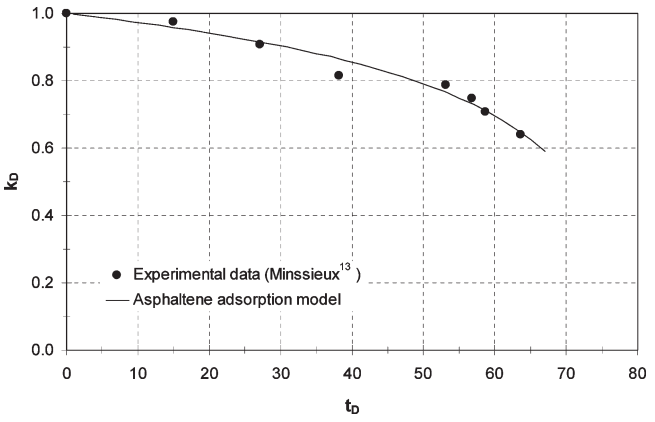

Figure 10. Comparison between experimental results obtained by Minssieux[13] (Run GF 1) and those generated with asphaltene adsorption model. $C_0 = 0.00125$ and $\lambda = 10$.

contains 5.3 wt % of asphaltenes, viscosity of 13 cP at 20 °C, 29°API, and it was displaced through the porous medium at a injection rate of 50 mL/h. This kind of rock was selected as a homogeneous model porous medium with regular grain size and morphology (pure silica and no clay present). As can be seen in Figure 10, core damage progressed according to a more-or-less slow process showing the evolution of oil permeability as a function of pore volumes of the dead crude oil. Parameters λ and C_0 from eq 6 were determined by trial and error. As can be seen from Figures 9 and 10, our model of asphaltene adsorption is in good agreement with the experimental data.

3.5.2. Process of Entrapment of Asphaltenes. This process is quite different to that previously discussed. The mechanism of asphaltene particles retention is due to being trapped at pore throats. As a result, this mechanism occurs when asphaltene particle diameter is comparable (or larger) to the pore throat diameter to cause a reduction of permeability. The dynamics of this process is described by the mass balance equations developed previously and applied when asphaltene particles diameter is the same size; thus

$$\frac{\partial c_{sD}}{\partial t_D} + \frac{\partial c_{sD}}{\partial x_D} = -\frac{1}{\mu} c_{sD} \frac{I_D(1/A)}{I_D(\infty)} \tag{7}$$

$$\frac{\partial N_{pD}}{\partial t_D} = -\frac{B}{\mu} c_{sD} \frac{I_D'(r_{pD})}{I_D(\infty)} \tag{8}$$

where $A = r_p^*/r_s^*$, $B = \phi c_s^*/N_p^*$, $\mu = l_p/L$, and I is an integral; r_p^* and r_s^* are average pore radius and asphaltene radius, respectively; c_s^* and N_p^* are characteristic asphaltene concentration and number of pores, respectively. r_{pD} is pore radius, l_p is average pore length, and L is length of the porous medium. If we assumed that the asphaltene particles distribute themselves in the pores in the same proportion as in the reservoir fluid, then the fraction of particles approaching unblocked pore throats in the size interval is proportional to the corresponding flow rate partition,[64] that is,

$$\frac{N_{pD} f_{pD} r_{pD}^2 u_{RD}\, dr_{pD}}{\int_0^\infty N_{pD} f_{pD} r_p^2 u_{RD}\, dr_{pD}} = \frac{I_D'\, dr_{pD}}{I_D(\infty)} \tag{9}$$

where it was denoted that,

$$I'(r_{pD}) = \int_0^{r_{pD}} u_{RD} r_{pD}'^2 f_{pD}\, dr_{pD}' \tag{10}$$

where u_{RD} is the fluid velocity through the pore throat. It must be noticed that the ratio $[I_D'(r_{pD})]/[I_D(\infty)]$ gives the fraction of rate flowing in pore throats in a pore radius range from zero to r_{pD} with respect to the total rate in the whole porous medium volume. Making eq 7 to be equal to eq 8, we obtained the following expression[66]

$$\frac{\partial (N_{pD} F_{pD})}{\partial t_D} = \frac{\partial N_{pD}}{\partial t_D} \tag{11}$$

Considering a change of variable of the form $z = x_D - vt_D$; where v is a constant to be determined. Finally, applying the following suitable boundary conditions:

$$c_{sD} = 0; \quad N_{pD} = 1 \tag{12}$$

$$c_{sD} = 1; \quad N_{pD} = a \tag{13}$$

From appropriate considerations it is possible to obtain the following expression for permeability reduction due to asphaltenes trapped process at pore throats,

$$k_D(t_D) = \frac{1}{\left(\frac{1}{k_1} - 1\right) v t_D + 1} \tag{14}$$

With k_1 being the permeability left behind of the asphaltene deposition front in the porous medium; v is the velocity of that front. Thus, it is relatively easy to determine when the permeability obeys a behavior similar to eq 14 because such deposition front will reach a limit at $x_D = 1$ (whole length of the porous medium), and k_1 can be considered as a constant. Therefore, it is possible to infer v and k_1 with enough experimental data in core tests; v can be estimated with the following expression:

$$v = \frac{1}{t_c} \tag{15}$$

where t_c is time, from this time permeability no suffer any alteration. We used experimental data in core tests reported by Minssieux,[13] Shedid,[16] and Ali and Islam[14] to validate the mathematical model developed in this work to represent the precipitated asphaltene trapped process. Figures 11−13 show the experimental data reported in the literature and those obtained by eq 14. As can be seen, our proposed model fitted satisfactorily the experimental data in the core test. In the case of the data in Figure 11, Minssieux[13] carried out a core test (RUN GV5) in a clayey sandstone with the asphaltene-rich (5.3 wt %) Weyburn crude (viscosity of 13 cP at 20 °C, 29°API, injection rate of 10 mL/h) as an example of drastic plugging mechanism caused by in situ accumulation or bridging of asphaltene trapped particles or asphaltene aggregates suspended in the crude oil. On the other hand, Shedid[16] performed a series of core test in order to study the influence of asphaltene precipitation on carbonate reservoirs rocks. The results (Figure 12) indicated that asphaltene precipitation damages absolute permeability and reduces effective porosity for different asphaltene contents (0.06−1.50 wt %) of crude oil flowing through carbonate cores. Specifically, the proposed model in this work was compared with the experimental data of the system crude oil (0.06 wt % of asphaltene) and carbonate core (initial absolute permeability of 6.67 mD, and initial effective porosity of 16.34%, injection rate of 1 mL/min).

(66) Sharma, M. M.; Yortsos, Y. C. *AIChE J.* **1987**, *33* (10), 1654–1662.

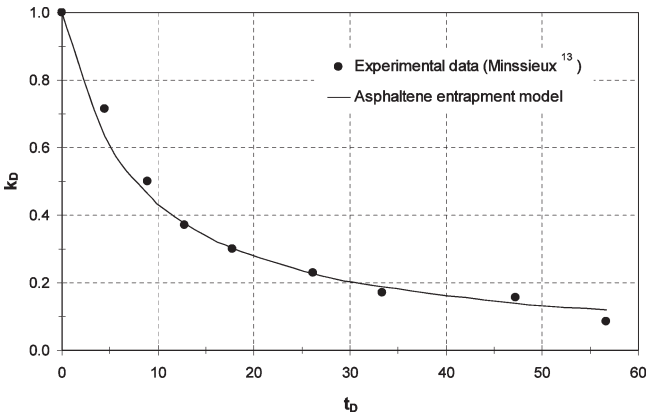

Figure 11. Comparison between experimental results obtained by Minssieux[13] (Run GV 5) and those generated with the asphaltene entrapment/trapped model. $C_1 = 0.13$.

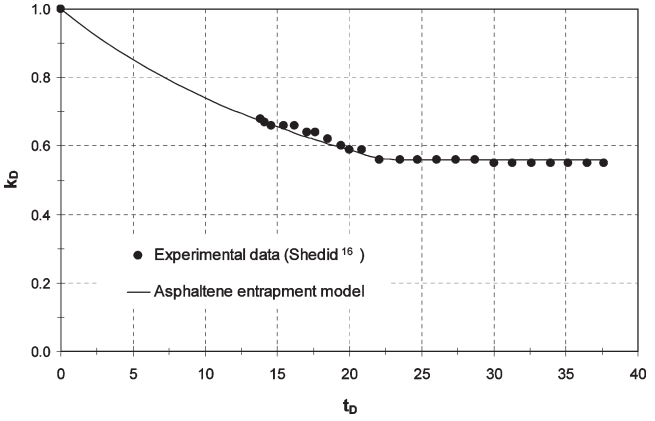

Figure 12. Comparison between experimental results obtained by Shedid[16] (Core 1) and those generated with the asphaltene entrapment model. $C_1 = 0.035$.

Finally, Ali and Islam[14] carried out a set of experiments to determine the effect of asphaltene adsorption and precipitation in low-permeability of carbonate rocks (Figure 13). They used a dead crude oil with a viscosity of 5.27 cP (29.29°API) and the asphaltene content was 3 wt %. As porous media, they used powdered limestone prepared by crushing and sieving limestone cores collected from local formations. The deasphaltene crude was injected through the porous media (effective porosity of 35%, initial permeability of 11.13 mD) at a rate of 0.5 mL/min until the pressure drop was stabilized.

It is important here to point out that we assumed the adsorption mechanism reduces the core permeability but no so drastically as it is caused by the plugging mechanism. In addition, it is well-known that the contribution of adsorption to the total amount of asphaltenes deposition is typically small and that the mechanical entrapment appears to be dominant.[67] In order to apply the adsorption model to the experimental data in Figures 9 and 10, we also considered two main ways that are features of the adsorption mechanism on the tested cores: (1) trend of the permeability behavior as a function of pore volume (curve shape: convex angle), and (2) various pore volumes are required to reduce the absolute permeability to a considerable extent. From Figures 9 and 10, we observed that the pore volumes

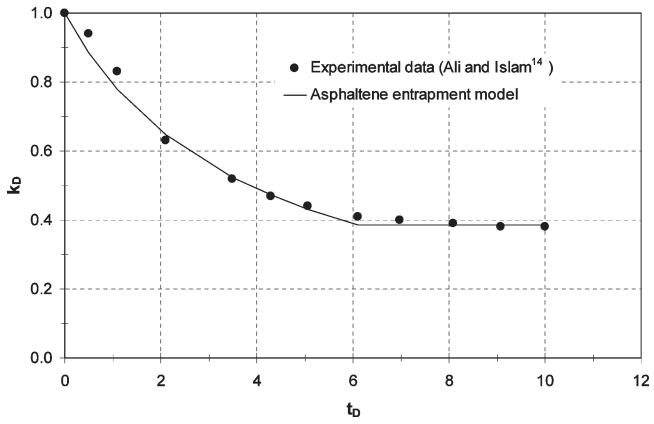

Figure 13. Comparison between experimental results obtained by Ali and Islam[14] and those generated with the asphaltene entrapment model. $C_1 = 0.26$.

required to reduce permeability were larger than 500 and 60, respectively. Analyzing Figure 11, is possible to observe that the permeability reduction was severe at a small certain value of t_D (corresponding to $k_D \approx 0.1$); it should be noticed that, for a similar value of t_D (around 60) in Figure 10, the absolute permeability was reduced not so rapidly ($k_D \approx 0.7$) as in Figure 11 in which we considered the plugging as the predominant mechanism (curve shape: concave angle). On the basis of these observations, it appears that for each mechanism considered as formation damage, the curve shape is distinct depending of the applied model. Thus, the two models selected here were used in order to support the interpretation of adsorption and plugging effects related to asphaltene deposition in porous media.

3.5.3. Coupling of Both Mechanisms. As mentioned previously, we assumed that first a gradual and slow reduction of core permeability occurs due to adsorption process, and then a plugging process develops in the pore throats. Thus, it is expected that eq 6 describes permeability reduction in the early time during the injection of crude oil containing asphaltene particles, and subsequently the permeability behavior described by eq 14, corresponding to the trapping process. It must be pointed out that, in these two models, we assumed that asphaltene particles have the same average size. This hypothesis could be an unrealistic condition; however, Leontaritis[68] demonstrated that asphaltene particles distribution (at least in tank oil conditions) is close to a gamma distribution, and for all practical purposes it can be considered unimodal.

Equation 14 was modified in order to adjust the time in which the trapping process starts. This time was established as t_0, and it was also obtained by trial and error. Finally, eq 14 was established as:

$$k_D = \frac{1}{C_1(t_D - t_0)+1} \tag{16}$$

where C_1 is equal to,

$$C_1 = \left(\frac{1}{k_1} - 1\right) v \tag{17}$$

From this approximation, there are four basic parameters (C_0, C_1, λ, and t_c) describing, along with the equations previously developed, the permeability change with respect

(67) Leontaritis, K. J., Asphaltene near-wellbore formation damage modeling. In SPE 39446 presented at the 1998 SPE Formation Damage Control Conference held in Lafayette, Louisiana, February 18−19.

(68) Leontaritis, K. J. Quantification of asphaltene and wax sludge build-up in crude oil storage facilities. In SPE 92958 presented at the SPE International Symposium on Oilfield Chemistry held in Houston, Texas, U.S.A., February 2−4, 2005; p 1.

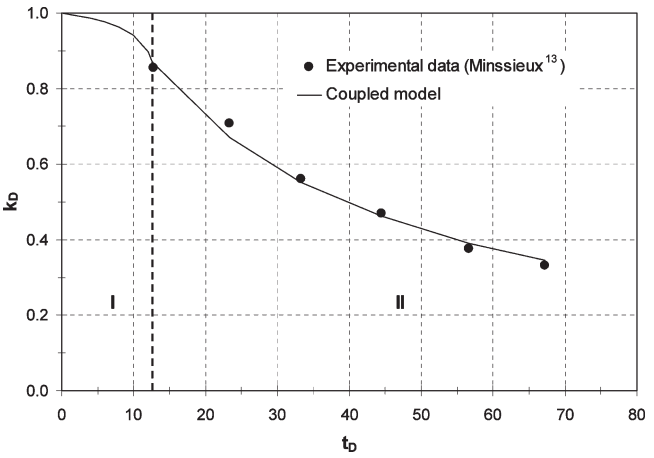

Figure 14. Comparison between experimental results obtained by Minssieux[13] (Run GF 3) and those generated with the coupled model. $C_0 = 0.07$; $C_1 = 0.032$; $\lambda = 50$; $t_c = 8$; I: adsorption process; II: plugging process.

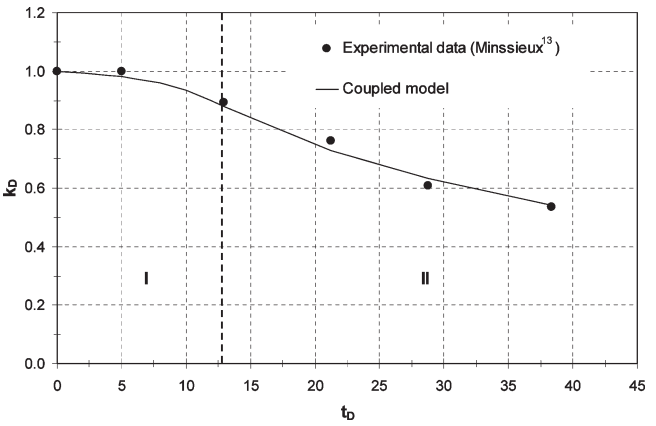

Figure 15. Comparison between experimental results obtained by Minssieux[13] (Run GP 9) and those generated with the coupled model. $C_0 = 0.07$; $C_1 = 0.032$; $\lambda = 50$; $t_c = 8$; I: adsorption process; II: plugging process.

to time. Thus, a new theoretical model is proposed in order to couple asphaltene adsorption with mechanical plugging due to the deposition process. This coupled model was applied to the experimental data reported by Minssieux[13] in core tests taking in account both mechanisms; it is shown from Figures 14 and 15 that permeability reduction during pressure depletion in a porous medium can be satisfactorily matched using this model. Finally, the coupled model results agree favorably with experimental results obtained in this work for which different flow rates were used (Figure 16).

It must be mentioned that the experimental procedure carried out at reservoir conditions using live crude oil (Figure 16) is very similar to those with dead crude oil (Figures 9−15). In other words, involved mechanisms affecting core permeability are basically the asphaltene adsorption and trapping processes. From Figures 9−16 it was observed that permeability reduction follows a similar trend with formation damage caused by solid fines migration.[13] From all the experimental data in cores test analyzed here, we observed that there exists a clear difference in core permeability reduction when (i) asphaltene precipitation is induced by a precipitating agent (n-peptane, n-heptane, etc.) using a dead crude oil[14,16,19,29,69] or using crude oils with different asphaltene content,[13] and (ii) asphaltene precipitation is induced by pressure depletion using a live crude oil or recombined oil.[69,70] This work demonstrated that the existence state of asphaltene in crude oil (Figure 7) is quite different than in solvent as most studies carried out in laboratory involving some aspects of asphaltene precipitation and deposition in reservoirs during primary oil recovery. From this study, we found that core permeability reduction by mechanical trapping process is slower or gradual when live crude oil or recombined oil is used (see Figure 7); however, it is necessary to perform more experiments (enough volume of live crude available for experiments) in order to confirm this assumption. Thus, the reservoir fluid containing asphaltene is a real solution, but asphaltene forms aggregation in solvent.[56]

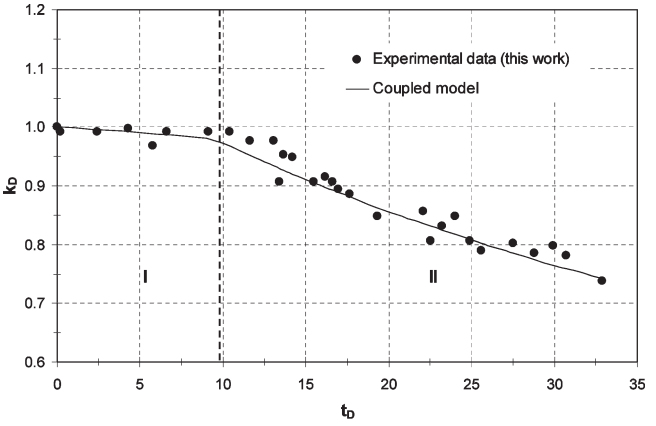

Figure 16. Comparison between experimental results obtained in this work and the coupled model developed. $C_0 = 0.04$; $C_1 = 0.014$; $\lambda = 50$; $t_c = 8$.

Conclusions

A dynamic displacement experiment with a live crude oil was carried out to determine the effect of in situ asphaltene precipitation and deposition by pressure depletion on petrophysical properties of a consolidated Bedford limestone rock. Live crude oil permeability measurements were shown to be stable inside APE upper boundary and by above the bubble-point pressure, at the study temperature. At near bubble-point pressure, asphaltene deposition diminished oil permeability by 24% of initial oil permeability with nearly 13 pore volumes of live crude oil injection; the effective porosity was decreased in 20%. Various pore volumes injected resulted in increased pore plugging of the core, causing increased reduction in absolute permeability. This works provided evidence that asphaltenic oil flow through a core sample can cause oil permeability reduction. Sufficient oil throughput is necessary in the laboratory in order to observe and follow the asphaltene plugging process resulting from in situ organic material deposition.

A mathematical model for asphaltene deposition in porous media, at a level for core test, was developed and validated directly though the use of laboratory data on core flow obtained of this investigation, as well as those found in the literature. Two distinct mechanisms were identified as a result of the precipitation and deposition processes, namely, asphaltene adsorption and mechanical trapping on the porous

(69) Holmes, K.; Potter, G.; Scott, D.; Williams, W.; Fate, T. Making successful permeability measurements with asphaltic crude oils. In International Symposium of the Society of Core Analysts, September 23−25, 2002; Vol *10*, p 1.

(70) Argüelles-Vivas, F. J. Efecto de la depositación de asfaltenos en el flujo de fluidos en medios porosos. *Tesis de Licenciatura*; Universidad Autónoma Metropolitana (UAM-A): 2006.

medium. A satisfactory qualitative agreement was observed with the experimental results.

Appendix

As a first approximation,[71] we have the following dimensionless mass balance equations:[64]

$$\frac{\partial}{\partial t_D}(c_{sD}f_{sD})+\frac{\partial}{\partial x_D}(c_{sD}f_{sD}) = (1-\theta)\mathrm{ER}c_{AD}f_{AD}-\theta\mathrm{ER}c_{sD}f_{sD}-\frac{I_D(r_{sD}/A)}{\mu I_D(\infty)}c_{sD}f_{sD} \quad (A1)$$

$$\frac{\partial}{\partial t_D}(c_{AD}f_{AD}) = -(1-\theta)\mathrm{ER}c_{AD}f_{AD}+\theta\mathrm{ER}c_{sD}f_{sD} \quad (A2)$$

$$\frac{\partial}{\partial t_D}(N_{pD}f_{pD}) = -\frac{B}{\mu}\frac{I_D'(r_{pD})}{I_D(\infty)}c_{sD}[1-F_{sD}(r_{pD}A)] +\theta c_o N_{pD}c_{sD}\frac{\partial}{\partial r_{pD}}\left[f_{pD}\left(\frac{u_{RD}}{r_{pD}}\right)^{1/3}\right] \quad (A3)$$

$$\frac{\partial}{\partial t_D}(c_{TD}f_{TD}) = \frac{I_D(r_{sD}/A)}{\mu I_D(\infty)}c_{sD}F_{sD} \quad (A4)$$

It is well-known that with the application of these equations to various processes, some of the terms become negligibly small. In particular, filtration processes are typically characterized by $\theta = 1$ (particle deposition), $A \gg 1$, while fines migration processes correspond to $\theta = 0$ (particle release), $A = 0(1)$. Following Sharma and Yortsos,[64,72] we take $r_p^* \gg r_s^*$, thus $A \gg 1$ and the integral $I_D(r_{sD}/A)$ becomes negligible for all but a negligibly small fraction of the injected particles [$I(r_{sD}/A) \ll 1$]. Similarly, the corresponding rates of pore closure due to size exclusion are negligibly small, as $r_{pD}A \gg 1$, hence $F_{sD}(r_{pD}A) = 1$.

Examination of the mass balances shows that the surviving rate terms do not explicitly involve the particle size distribution f_s; thus, eqs A1, A2, and A3 may integrate over all asphaltene particles sizes to obtain

$$\frac{\partial}{\partial t_D}(c_{sD}f_{sD})+\frac{\partial}{\partial x_D}(c_{sD}f_{sD}) = -ERc_{sD}f_{sD} \quad (A5)$$

$$\frac{\partial}{\partial t_D}(c_{AD}f_{AD}) = ERc_{sD}f_{sD} \quad (A6)$$

$$\frac{\partial}{\partial t_D}(N_{pD}f_{pD}) = c_o N_{pD}c_{sD}\frac{\partial}{\partial r_{pD}}\left[f_{pD}\left(\frac{u_{RD}}{r_{pD}}\right)^{1/3}\right] \quad (A7)$$

$$\frac{\partial}{\partial t_D}(c_{TD}f_{TD}) = 0 \quad (A8)$$

where the dimensionless subscript D has been introduced for convenience. Equations A5, A6, and A7 describe the local behavior of the filtration/adsorption process based on the model postulates of mass-transfer limited regime and constant injection/flow rate and porosity premises. Before we proceed with the solution of the above equations, we note that in eq A5 the term ER represents a local dimensionless filtration/adsorption coefficient. We identify[69]

$$\lambda \propto \mathrm{ER} \quad (A9)$$

In the course of filtration/adsorption, additional effects of the process parameter on the local filtration/adsorption coefficient enter implicitly through the dimensionless parameter c_o. Equations A5, A6, A7, and A9 also suggest that the local filtration/adsorption coefficient is a function of time and distance along the filter bed or porous media, through the parameter c_o. Assuming that all asphaltene particles is the same size, that is, f_{sD} is a constant; thus, eqs A5 and A6 can be rewritten as

$$\frac{\partial c_{sD}(x_D,t_D)}{\partial t_D}+\frac{\partial c_{sD}(x_D,t_D)}{\partial x_D} = -\lambda c_{sD}(x_D,t_D) \quad (A10)$$

$$\frac{\partial}{\partial t_D}(N_{pD}f_{pD}) = c_0 N_{pD}c_{sD}(x_D,t_D)\frac{\partial}{\partial r_{pD}}\left[f_{pD}\left(\frac{u_{RD}}{r_{pD}}\right)^{1/3}\right] \quad (A11)$$

In order to solve eq A11, it is necessary to determine the term $c_{sD}(x_D,t_D)$ from eq A10. Thus, applying the Laplace transform to eq A10 and taking in account the following initial and boundary condition

$$c_{sD}(x_D, t_D = 0) = 0 \quad (A12)$$

$$c_{sD}(x_D = 0, t_D) = 1 \quad (A13)$$

and some algebraic operations, it is possible to obtain

$$\frac{\partial}{\partial x_D}C_{sD}(x_D,s) = -(\lambda+s)C_{sD}(x_D,s) \quad (A14)$$

Applying separation of variables to eq A14 and integrating both sides with respect to x_D ($0 \le x_D' \le x_D$), we have

$$C_{sD}(x_D,s) = C_{sD}(x_D = 0,s)e^{-(\lambda+s)x_D} \quad (A15)$$

Now, taking into account the boundary condition and applying the Laplace transform to eq A13, we obtain

$$C_{sD}(x_D = 0,s) = \frac{1}{s} \quad (A16)$$

Substituting eq A16 into eq A15, and applying the inverse Laplace transform to eq A15, then we have

$$c_{sD}(x_D,t_D) = e^{-\lambda x_D}H(t_D-x_D) \quad (A17)$$

Assuming a unimodal distribution function of pore throat size (f_p) to be equal to the conductance distribution (f_g also unimodal); thus,

$$f_{pD} = f_g = \delta(r_{pD}-r_{pD}^*) = \delta(g-g_m) \quad (A18)$$

and introducing the following relationships[64,69]

$$g = r_{pD}^4 \quad (A19)$$

$$k_D = \frac{k}{k_0} = \frac{g_m}{g_{mo}} \quad (A20)$$

$$r_{mD} = g_m^{1/4} \quad (A21)$$

(71) Matías-Pérez, V. Desarrollo de un modelo matemático para caracterizar e identificar el tipo de daño a la formación causado por depositación de asfaltenos. *Tesis de Maestría*; Universidad Nacional Autónoma de México: 2009.

(72) Sharma, M. M.; Yortsos, Y. C. *AIChE J.* **1987**, *33* (10), 1644–1653.

Substituting eqs A20, A19, and A21 into the term u_{RD}, eq A7 and making $(Z/2) - 1 = \alpha$, we obtain

$$u_{RD} = \frac{r_{pD}^2}{8k_D}\left[1+\frac{r_{mD}^4 - r_{pD}^4}{r_{pD}^4+(Z/2-l)r_{mD}^4}\right] = \frac{g_{mo}g^{1/2}}{8g_m}\left[\frac{g_m(1+\alpha)}{g+\alpha g_m}\right] \quad (A22)$$

From eq A19 and some mathematical operations,

$$\frac{\partial}{\partial r_{pD}} = 4g^{3/4}\frac{\partial}{\partial g} \quad (A23)$$

Now, substituting eqs A18, A22, and A23 into eq A11 and integrating with respect to g, then

$$\frac{\partial}{\partial t_D}\int_0^\infty g\delta(g-g_m)dg = 2c_o c_{sD}(x_D,t_D)\left(\frac{g_{mo}}{g_m}\right)^{1/3} \int_0^\infty g^{7/4}\frac{\partial}{\partial g}\left\{\delta(g-g_m)g^{1/12}\left[\frac{g_m(1+\alpha)}{g+\alpha g_m}\right]^{1/3}\right\} dg \quad (A24)$$

Making use of the Dirac delta function, g_m is related with the conductance distribution by means of the relationship

$$g_m = N_{pD}\int_0^\infty g f_g\, dg = \int_0^\infty g\delta(g-g_m)\, dg \quad (A25)$$

Then, eq A24 can be simplified to

$$\frac{\partial g_m}{\partial t_D} = 2c_o c_{sD}(x_D,t_D)\left(\frac{g_{mo}}{g_m}\right)^{1/3} g_m^{1/12} \int_0^\infty g^{7/4}\frac{\partial}{\partial g}\{\delta(g-g_m)\}\, dg \quad (A26)$$

Considering the following expression

$$\delta(g-g_m) = \delta_{g_m}(g) \quad (A27)$$

From eq A27 is possible to obtain

$$\frac{\partial}{\partial g}\delta_{g_m}(g) = -\frac{1}{g}\delta_{g_m}(g) \quad (A28)$$

Substituting eqs A27 and A28 into eq A26, we have

$$\frac{\partial g_m}{\partial t_D} = -2c_o c_{sD}(x_D,t_D)g_{mo}^{1/3}g_m^{1/2}\int_0^\infty \delta_{g_m}(g)\, dg \quad (A29)$$

and taking into account the following

$$\int_0^\infty \delta_{g_m}(g)\, dg = \int_0^\infty \delta(g-g_m)\, dg = 1 \quad (A30)$$

Substituting eq A30 into eq A29 and applying separation of variables, we obtain

$$\frac{1}{2}\frac{dg_m}{g_m^{1/2}} = -c_o c_{sD}(x_D,t_D)g_{mo}^{1/3}\, dt_D \quad (A31)$$

Substituting eq A17 into eq A31 and integrating from $g_{mo} \le g'_m \le g_m$ and $x_D \le t'_D \le t_D$, then

$$\frac{1}{2}\int_{g_{mo}}^{g}\frac{dg'_m}{g'^{1/2}_m} = -c_o e^{-\lambda x_D}g_{mo}^{1/3}\int_{x_D}^{t_D} H(t_D-x_D)\, dt'_D \quad (A32)$$

and making use of the Heaviside function, we obtain

$$\left(\frac{g_m}{g_{mo}}\right) = [1-c_o g_{mo}^{-1/6}e^{-\lambda x_D}(t_D-x_D)]^2 \quad (A33)$$

Finally, the effective permeability [eq A20] can be determined as a harmonic mean given by

$$k_D(t_D) = \frac{1}{\int_0^1[(dx_D)/[1-C_0 e^{-\lambda x_D}(t_D-x_D)]^2]} \quad (A34)$$

Acknowledgment. The contribution of Alfredo Ríos Reyes (Laboratorio de Productividad de Pozos, Área de Termodinámica de Altas Presiones) in measuring the APE upper boundary as well as bubble-point pressure experiments is gratefully acknowledged. This research was supported by the Instituto Mexicano del Petróleo under Projects D.31519 and D.00506.